Supporting Information

Datta et al. 10.1073/pnas.1602789113

SI Materials and Methods

Details of Animals Used. Except where otherwise noted, all mice were male or female SPF or GF C57BL/6 mice between 2–6 mo of age, fed a standard solid chow diet and given ad libitum access to water. The GF chow was autoclaved and was formulated to have a nutritional profile after autoclaving similar to that of the SPF chow. The mice given only sucrose or only sucrose + PEG were first raised on a standard solid chow diet and given ad libitum access to water then maintained on a restricted diet consisting only of 5% (wt/vol) sucrose or 5% (wt/vol) sucrose + 7% (wt/vol) PEG 200k in 1× PBS (pH 7.4, without calcium and magnesium; Corning) available for ad libitum consumption for the 24-h period before they were euthanized. Four hours after we started administering each of the restricted liquid diets we moved each test mouse to a new, clean cage to minimize the effects of coprophagy.

Details of Microscopy. All imaging was performed using a Zeiss LSM 510 upright confocal microscope or a Zeiss LSM 880 upright confocal microscope, using either bright-field microscopy, confocal fluorescence microscopy (543-nm excitation/560-nm long-pass filter or 488-nm excitation/505-nm long-pass filter), confocal reflectance microscopy (514-nm excitation/505-nm long-pass filter or 505- to 735-nm detection), or two-photon microscopy (800-nm excitation/650-nm long-pass filter). We collected 3D stacks consisting of multiple *xy* slices at different *z* positions.

Imaging of Unwashed Tissue. We euthanized each mouse, removed the colon, and immediately flushed it gently with Fluorinert FC 40 oil (3M), which is immiscible with the aqueous contents of the colon. We then immediately cut the colon segment open along the longitudinal axis and mounted the opened tissue (luminal surface facing upward) onto a glass slide or a Petri dish using GLUture topical tissue adhesive (Abbott). We then gently deposited ∼0.5–2 mL of additional FC 40 oil onto the exposed luminal surface. The FC 40 is immiscible with water and with the mucus hydrogel; this procedure thus retained the adherent mucus in its in vivo "unwashed" state and prevented it from dehydrating. We imaged the explant with two-photon microscopy. For some mice, we took multiple explant samples and for some explant samples we collected multiple 3D stacks at different fields of view.

We determined the mean mucus thickness (gray bars in Figs. 1 and 4) for each stack obtained from an explant by measuring the distance between the epithelial surface (Fig. S1 *A* and *B*) and the FC oil–hydrogel interface at five random positions in *xy*. In some cases this was repeated for multiple fields of view. When multiple colonic explants were obtained from a single mouse, we calculated the mean mucus thickness of an individual mouse. In Figs. 1 and 4, the thickness values reported are the mean values of the individual mice thicknesses. The error bar on each value reported in Figs. 1 and 4 is the SEM, calculated by taking the SD of mucus thickness for a single mouse and dividing by $\sqrt{n}$ (n, number of different mice).

Imaging of Washed Tissue. We euthanized each mouse, removed the colon, and immediately flushed it gently with ice-cold 1× PBS and placed ∼1-cm-long segments of the midcolon in ice-cold PBS, ensuring that the ionic composition was homogenized throughout the mucus hydrogel environment. We then cut and mounted the colon segments as described for unwashed tissues, always ensuring the explant surface was covered in PBS to prevent any dehydration or ionic imbalance, and surrounding (but not contacting) the tissue with >10 ∼10-μL drops of water to maintain a humid environment. The measured mucus hydrogel thickness was consistent with the distance measured when we imaged using FC oil and consistent with other reported measurements (8), did not change appreciably over an observation time of 2.5 h, and was similar for probes of other sizes (250 nm in diameter or larger), as discussed in the main text, further confirming the validity of our approach. We then gently deposited an additional ∼10- to 200-μL drop of test solution containing the fluorescent probes onto the explant. We imaged the explant with confocal reflectance or two-photon microscopy. For some mice, we took multiple explant samples and for some explant samples we collected multiple 3D stacks at different fields of view. The levels of the images in Fig. 2*A* were nonlinearly adjusted in Adobe Illustrator for clarity in print using the following input and output levels: 82, 1, 246/0, 255 (bright field), 34, 0.78, 172/0, 205 (confocal reflectance), and 51, 0.91, 140/0, 255 (two-photon).

Thickness Measurements of Washed Mucus Hydrogel. In each experiment, after placing a suspension of 1-μm-diameter microparticles onto the exposed luminal surface, we incubated the tissue at 4 °C for 1–2 h, longer than the time required for the microparticles to diffuse across the vertical extent of the mucus in free solution (40 min). This ensured that the microparticles deposited onto the mucus hydrogel surface. We simultaneously imaged both the epithelium and the deposited microparticles using bright-field, confocal reflectance, or two-photon reflectance microscopy.

To determine the mean mucus thickness for tissue obtained from a single mouse (green, light blue, dark blue, and pink points in the bottom graph of Fig. 2*D*), for each stack on a washed explant we measured the distance between the epithelial surface and the center of the deposited microparticles at five random positions in *xy* spanning the entire field of view. In some cases this process was repeated for multiple fields of view. If multiple colonic explants were obtained from the same mouse, the thickness was measured in the same way. We then took each of these individual thickness measurements at each *xy* position from all of the individual mice, explants, and fields of view and calculated the mean and SD. The thickness values reported in Fig. 2*D* are these mean values, and the error bars are the associated SD. The washed values and error bars reported Fig. 4 (purple bars), were determined as described in *Materials and Methods*, *Imaging of Unwashed Tissue*.

Experiments with Probes of Different Sizes. We used (all in 1× PBS) methoxyl polyethylene glycol-FITC (mPEG-FITC; Nanocs), weight-averaged molecular weight 350, 1.2×10^{-2} mg/mL; mPEG-FITC (Nanocs), weight-averaged molecular weight 5 kDa, 3.3×10^{-2} mg/mL; mPEG-FITC (Nanocs), weight-averaged molecular weight 200 kDa, 0.6 mg/mL; FITC–dextran (Sigma-Aldrich), average molecular weight 2 MDa, 0.1 mg/mL; and fluorescent polystyrene microparticles (micromer; micromod Partikeltechnologie GmbH), coated with PEG 300 to render them chemically inert (41), 0.02–0.2% volume fraction of manufacturer-reported average diameters 100 nm, 250 nm, 500 nm, 1 μm, or 5 μm. Penetration measurements used fluorescently labeled polymers at concentrations below those that cause mucus compression.

We characterized probes or polymers 500 nm or smaller using dynamic light scattering performed on 200–500 μL of each sample with a Wyatt Dynapro NanoStar instrument. The data were collected and analyzed using Wyatt DYNAMICS software 7.1. Hydrodynamic radii were determined by fitting the data using a regularization analysis. The wavelength of the laser was 658 nm and the scattering angle was 90°. The microparticle

solutions were unfiltered, whereas we filtered the polymer solutions using either a 0.2-μm Fisherbrand (PEG 400, PEG 6 kDa, PEG 200 kDa, fluorescent PEG 200 kDa, fluorescent dextran 2 MDa, and fluorescent PEG 5 kDa) or a 0.45-μm Puradisc (pullulan and dextrin) syringe filter. All samples were dispersed in 1× PBS, and we used the following concentrations or volume fractions: 3 mg/mL (fluorescent PEG 200 kDa), 1 mg/mL (fluorescent dextran 2 MDa), 0.1% (vol/vol) (100-nm particles), 0.01% (vol/vol) (250-nm particles), 0.02% (vol/vol) (500-nm particles), 100 mg/mL (PEG 400), 10 mg/mL (PEG 6 kDa), 0.5 mg/mL (PEG 200 kDa), 10 mg/mL (pullulan), 10 mg/mL (dextrin), and 0.25 mg/mL (fluorescent PEG 5 kDa). The acquisition time was 5 s, and 10–20 acquisitions were taken for each sample. We characterized the 1-μm and 5-μm microparticles using optical microscopy.

Polymers Used for Compression Measurements. We used (all in 1× PBS) PEG 400, weight-averaged molecular weight 380–420 Da (Acros Organics); PEG 6k, weight-averaged molecular weight 5.6–6.6 kDa (Acros Organics); PEG 200k, viscosity-averaged molecular weight 200 kDa (Sigma-Aldrich); dextrin, average molecular weight between ∼1–70 kDa (42–45) (Walgreens); pullulan from *Aureobasidium pullulans*, average molecular weight between ∼50 kDa and 4 MDa (46–50) (Sigma-Aldrich); and pectin from apple, weight-averaged molecular weight ∼100 kDa (51) (Sigma-Aldrich). We estimated the average radius of gyration, $R_{g,p}$, of the PEG 400, 6k, and 200k as ∼0.7, 3, and 22 nm, respectively, using published measurements (52) and our own dynamic light scattering measurements.

Quantifying Polymer-Induced Compression of Washed Mucus Hydrogel. After measuring the initial washed mucus thickness, we gently deposited ∼0.2–2 mL of the test polymer solution onto the exposed luminal surface and then collected the same 3D stacks at the same *xy* fields of view. To measure the "percent compression," or the overall percentage change in the thickness, of the colonic mucus after exposure to the polymer solution, we measured the thickness before and after exposure to the solution at the same five *xy* positions, using the distance between the epithelial surface and the deposited microparticles in the 3D stacks. To calculate the percentage compression, we calculated the percentage change in the thickness measured, as well as the measurement uncertainty (using the optical slice thickness as the experimental uncertainty in the measured thickness), at each of these five *xy* positions. We then calculated the percentage compression as the mean of these five measured values. The error bars show the uncertainty in the percentage compression measurement, which was calculated using the experimental uncertainty in each of the five strain measurements.

To explore the generality of the observed compression, we tested a number of different conditions and found similar behavior (as shown in Fig. 3*B*) for mice of different sexes and strains, for washed explants originating from GF or microbe-colonized mice, for different buffers (PBS or Hepes), for buffers also containing protease inhibitor, for polymer solutions prepared using the liquid fraction of SPF mice colonic contents instead of buffer, for experiments performed at 22 °C or 37 °C, for a similar, but charged, polymer, and in the presence and the absence of Mg^{2+} ions. We note that other multivalent cations (e.g., Ca^{2+}) have been found to induce additional structural changes in mucins, although no measurable changes were reported for Mg^{2+} (53). We also note that, in vivo, water may be absorbed from the lumen into the epithelium depending on the delivery medium (e.g., as reported in ref. 54). We speculate that this could concentrate the polymer in the lumen, possibly enhancing the mucus compression we measured ex vivo.

Flory–Huggins Model of Compression. We used the Flory–Huggins theory of polymer solutions to describe polymer interactions with the mucus hydrogel. The adherent mucus is a hydrogel with a network (10, 37, 55) composed of MUC2 proteins having alternating hydrophilic, densely glycosylated regions, which make up the strands of the hydrogel network, and hydrophobic, non-glycosylated regions, which help to cross-link the network, which is also cross-linked via physical entanglements, electrostatic interactions, and chemical cross-links such as disulfide bonds (56, 57). We therefore modeled the mucus as a cross-linked hydrogel swollen in a good solvent. For simplicity, we treated this hydrogel as being structurally isotropic; our model does not incorporate any possible supramolecular structuring of the colonic mucus hydrogel (37). We made the simplifying assumption that the mucus behaves as an elastic gel; although hydrogels, including colonic mucus, are known to be viscoelastic—they relax stresses over long times—the reversibility of the observed polymer-induced compression, and the observed unchanging thickness of the hydrogel after compression, suggest that the colonic mucus is elastic on the timescale of our experiments. This idea is supported by rheological measurements on a scraped porcine colonic mucus hydrogel, which exhibits elastic behavior for timescales of at least ∼100 s (58). Moreover, this assumption has been successfully used to describe the compression of synthetic hydrogels that also contain chemical cross-links (30, 31). However, we note that the exact details of mucus hydrogel rheology remain unknown; we therefore chose to describe the mucus hydrogel as "viscoelastic" in the text for the sake of generality, thereby including any possible elastic or viscous response. Incorporating further details of mucus hydrogel rheology into our theoretical model, such as any possible viscous relaxation at long timescales and the relative importance of the different forms of cross-linking in the network, will be an important direction for future work.

First, we calculated the total free energy of the ternary solvent–mucus–polymer system, G, given by the sum of the elastic free energy, G_{el}—which accounts for deformations of the individual mucus network strands, thus inhibiting the unphysical case of full mixing of the mucins and solvent—and the free energy of mixing the polymer and the solvent with the mucus hydrogel, G_m. The buffered aqueous solutions are characterized by a high ionic concentration (ionic strength ∼70 mM) and therefore a Debye screening length ∼0.7 nm, over two orders of magnitude smaller than the hydrogel mesh size, suggesting that electrostatic interactions may not play a significant role in our system. Indeed, theoretical predictions for charged semidilute polymer solutions reduce to those for uncharged semidilute polymer solutions when the solvent has a high ionic concentration such as ours (e.g., ref. 59). This idea is also supported by experimental measurements of charged particle diffusion in a mucus hydrogel, which show results similar to the case of uncharged particles at high ionic concentrations similar to ours (60). We therefore did not consider electrostatic effects (59, 61–64) in our work; considering these effects will be an interesting direction for future work.

The total change in free energy can thus be written as

$$\Delta G = \Delta G_m + \Delta G_{el} \qquad \text{[S1]}$$

and ΔG_m is given by the Flory–Huggins (30, 39, 40) free energy of mixing,

$$\Delta G_m = RT\left(\sum_i n_i \ln \nu_i + \sum_{i<j} n_i \nu_j \chi_{ij}\right), \qquad \text{[S2]}$$

where R is the gas constant, T is the temperature, n_i is the number of moles of species i, ν_i is the volume fraction of species i, and χ_{ij} is the Flory–Huggins interaction parameter between species i and j; here, we denote solvent, mucus, and free polymers as $i = S, M, P$, respectively. To describe the free energy of

elastic deformation we used rubber elasticity, assuming affine deformation of the network (30, 39):

$$\Delta G_{el} = \frac{3}{2}\frac{RT}{N_M V_S}\left[\left(\frac{\nu_M^0}{\nu_M}\right)^{2/3} - 1 - \ln\left(\frac{\nu_M^0}{\nu_M}\right)^{1/3}\right], \qquad \textbf{[S3]}$$

where ν_M is the mucus hydrogel volume fraction, ν_M^0 is the mucus hydrogel volume fraction in its initial preparation state, V_S is the molar volume of the solvent, and N_M is the average number of mucin Kuhn segments, the stiff segments making up each mucin network strand, between cross-links of the network. More sophisticated forms of the elastic free energy would be interesting to explore in future work; we note that the exact choice of the elastic energy may not affect the calculated hydrogel compression trends considerably (29, 30).

At equilibrium, the chemical potentials of both the solvent and the free polymer, $\mu_S \equiv \partial G/\partial n_S$ and $\mu_P \equiv \partial G/\partial n_P$, must be equal inside and outside of the mucus network:

$$\mu_S^{in} = \mu_S^{out} \qquad \textbf{[S4]}$$

$$\mu_P^{in} = \mu_P^{out}. \qquad \textbf{[S5]}$$

By substituting Eqs. **S2** and **S3** into Eq. **S1**, and differentiating with respect to the number of moles of solvent and free polymer, we obtained Eqs. **1**–**4** shown in the main text, which represent the central result of the Flory–Huggins model and have been successfully used to describe polymer-induced compression of synthetic hydrogels (30). These equations are also subject to the constraints $\nu_S^{in} + \nu_M + \nu_P^{in} = 1$ and $\nu_S^{out} + \phi = 1$.

We first treated the polymer-free case ($\phi = 0$), which describes the initial swollen state of the mucus hydrogel. The system is described by Eq. **1** with $\mu_S^{in} = \mu_S^{out} = 0$ and $\nu_P^{in} = 0$; this provided us with a relationship between ν_M^0, χ_{SM}, N_M, and the mucus volume fraction in this initial swollen state, which we denote as ν_M^s. Direct measurements of ν_M^s are lacking; we chose a value of $\nu_M^s = 0.01$, well within in the range of estimates (65–69) of the volume fraction of swollen mucus, and tested the sensitivity of our results to variations in the numerical parameters used, with the constraint relating ν_M^0, χ_{SM}, N_M, and ν_M^s (Fig. S9). As a simplifying assumption, we took ν_M^0 to be approximately equal to the mucin volume fraction when initially packed in secretory granules, before being released into the intestinal lumen to form the swollen, cross-linked adherent hydrogel. We found in our sensitivity analysis (Fig. S9) that our results are only weakly sensitive to the choice of the value of ν_M^0. We therefore chose a value $\nu_M^0 = 0.13$, within the range of published measurements (70–72) for mucin and other similar secretory granules. However, more work is required to quantitatively determine the exact value of ν_M^0. We expect water to be a good solvent for the mucin network strands, due to the preponderance of hydroxyl, carboxyl, and sulfate groups in the glycosylated domains; we therefore chose $\chi_{SM} = 0$. We estimated N_M using published measurements in two different ways. In the first approach, we used measured values (65, 73–76) of the MUC2 radius of gyration, $R_{g,M}$, and Kuhn length, b_M, combined with the relationship for mucus strands swollen in a good solvent (40, 68, 77, 78), $R_{g,M} \approx b_M N_M^{3/5}$. In the second approach, we used our direct measurements of the mucus hydrogel mesh size, combined with the published measurements of b_M, to estimate N_M. In both cases, we found $N_M \approx 20 - 10{,}000$. The values of ν_M^0, χ_{SM}, and ν_M^s, together with Eq. **1**, yielded $N_M \approx 1{,}000$, in this estimated range; we therefore chose $N_M = 1{,}000$. Again, we found qualitatively similar results for different values of N_M (Fig. S9).

We next investigated how added polymer ($\phi > 0$) changed the extent to which the mucus hydrogel is swollen, and therefore its equilibrium thickness. We numerically solved Eqs. **S4** and **S5** for ν_M and ν_P^{in}, varying ϕ; this yielded the curves presented in Fig. 3*A*. We focused on the case in which the added polymer is PEG 400, 6k, or 200k, as used in our experiments. We took the number of segments of each PEG, y, to be the number of PEG Kuhn segments, and estimated this (40) using the relationship $R_{g,P} \approx b_P y^{\alpha}$, where $R_{g,P}$ and b_P are the PEG radius of gyration and Kuhn length, respectively, choosing $\alpha = 0.58$, consistent with the measured range (40, 52, 79–82) $\alpha = 0.537 - 0.588$. Published measurements (83–85) yield $b_P \approx 0.76 - 1.8$ nm; we therefore chose $b_P = 1.28$ nm, in this range. We estimated $R_{g,P}$ using our measurements of the PEG 400, 6k, and 200k hydrodynamic radii and converted these to radii of gyration using the Kirkwood–Riseman relationship (86–88). The relationship between $R_{g,P}$, b_P, and y thus yielded y = 1, 4, and 146 for PEG 400, 6k, and 200k, respectively, which we used for the main simulations (Fig. 3*A*). Based on published measurements for PEG (30, 89), we set $\chi_{SP} = 0.45$. The chemical interactions between PEG and mucins are thought to be slightly attractive or neutral. We therefore estimated χ_{MP} to be between 0 and 0.5, and chose $\chi_{MP} = 0.3$.

This Flory–Huggins framework has been successfully applied to qualitatively describe polymer-induced compression of a number of synthetic hydrogels (30, 31, 90–94). However, it is a simple mean-field theory, does not take into account correlations between monomers, and assumes affine deformation of a homogeneous gel. We therefore did not expect strong quantitative agreement between the experiments and numerical calculations. However, we observed similar behavior between the two, using parameters that are consistent with experimentally measured values. In particular, the Flory–Huggins calculations showed that the free polymer does induce compression of the network, even though in the calculations the polymer could penetrate into the mucus hydrogel, and the trends we observed experimentally are qualitatively similar to those predicted by the model. Moreover, we found that polymers of higher molecular weights required a lower monomer volume fraction to compress the network, consistent with our experimental observations. One reason for this is the entropic penalty paid by PEG to penetrate the mucus; because this penalty is larger for larger polymers, they are more likely to be excluded from the mucus hydrogel, and therefore can compress it more by elevating the difference between external and internal osmotic pressure. Consistent with this expectation, we found that the higher-molecular-weight PEG was more likely to be excluded from the mucus hydrogel (Fig. S9*E*).

More sophisticated modeling could build on the work presented here by incorporating effects such as structuring of the colonic mucus hydrogel (37), viscoelastic relaxation of the mucus network, chemical adhesion (41) or electrostatic interactions, or polymer complex formation. For example, PEG has been observed to form complexes with polycarboxylic acids (30, 95–99), via hydrogen bonding between the ether oxygen of PEG and undissociated carboxylic groups; similar effects could play a role in our experimental system. We note, however, that at the physiological pH explored in our work the carboxyl groups found on the sialic acid residues of mucins are negatively charged (55, 57) and complexation is unlikely (Fig. S7).

Experiments Using Liquid Fraction of Colonic Contents. Immediately after euthanizing a mouse, we collected its colonic contents in a polypropylene spin column with a 30-μm-pore-size filter (Thermo Scientific Pierce), always kept on ice, and centrifuged at 17,000 × *g* for 100 min at 4 °C. We then collected the liquid supernatant from the collection tube. We combined the liquid fraction thus obtained from multiple mice, both male and female, 3–4 mo of age, to obtain enough sample for the experiments, and stored aliquots at −20 °C until experimental use.

To test whether luminal contents could affect the polymer-induced mucus compression reported here, we used our ex vivo

approach to also test compression induced by polymer solutions prepared in the thawed liquid fraction of SPF mice colonic contents instead of buffer. We tested both 3.1% (wt/vol) PEG 200k and 48.5% (wt/vol) dextrin, using the SPF liquid fraction as the solvent in both cases. In both cases, we verified that addition of the polymer to the SPF liquid fraction did not result in the formation of precipitates. In each case, we incubated a washed explant with 1-μm microparticles and used confocal reflectance microscopy to first measure the initial, washed mucus thickness. We then gently deposited 65–75 μL of the test solution on the exposed luminal explant surface and reimaged to measure the change in mucus thickness. We found that the mucus hydrogel compressed by 55 ± 2% in the case of PEG 200k and 52 ± 2% in the case of dextrin, similar to the compression measured for the same polymers in saline (as shown in Figs. 3*B* and 4*A*). This result suggests that additional luminal contents do not mask the effect of polymers in the gut. Further investigations along these lines will be an interesting extension of our work.

For each of the experiments shown in Fig. 4*C*, we incubated a washed explant with 1-μm microparticles and used two-photon microscopy to first measure the initial, washed mucus thickness. We then thawed the frozen liquid fraction of colonic contents, gently deposited 100 μL of it on the exposed luminal explant surface, and reimaged to measure the change in mucus thickness. We then obtained successive 3D stacks to verify that the thickness did not change in time over a time period of ∼10–30 min. We also collected multiple 3D stacks at different fields of view on the same tissue explant, and for different tissue explants obtained from multiple mice. The difference between the SPF and GF chromatograms in Fig. S10 suggested that, as expected (100–104), the GF contents were enriched in polymers of higher molecular weight compared with the SPF contents, and that these polymers were comparable in size to ∼200- to 700-kDa pullulan standards. As described in the main text, we found that the SPF contents did not appreciably compress colonic mucus, indicating that any residual polymers present in the SPF contents (after microbial degradation) were insufficient to compress the hydrogel; this result is also consistent with our observation that SPF mice and mice maintained on a sucrose diet had colonic mucus hydrogels of comparable thickness (Fig. 1, $P = 0.3$). By contrast, we found that the GF contents compressed colonic mucus by ∼70% of its initial washed thickness, for washed explants obtained from either SPF or GF mice (Fig. 4*C*). This finding indicates that gut microbes, by modifying the polymeric composition of intestinal contents, can actively modulate the compression state of the colonic mucus hydrogel (Fig. 4*D*).

Detailed contributions from noncorresponding authors:

A.P.S. codesigned all experiments and coanalyzed all experimental results; codeveloped theoretical tools and coperformed the experiments and calculations; performed some of the FC oil measurements and analyzed some of the results in Figs. 1 and S1; performed some of the ex vivo experiments and analyzed some of the results in Figs. 2–4 and S3–S7; codeveloped the theoretical model; cooptimized and coperformed calculations for the theoretical model and coanalyzed results in Fig. 3; performed a sensitivity analysis for the theoretical model shown in Fig. S9; performed dynamic light scattering measurements of polymers and probes; designed and performed GPC measurements in Fig. S10; cowrote the paper.

S.S.D. coplanned the project; codesigned all experiments and coanalyzed all experimental results; codeveloped theoretical tools and coperformed the experiments and calculations; set up polymer-fed animal experiments (Fig. 1); performed some of the FC oil measurements and analyzed some of the results in Figs. 1 and S1; developed the ex vivo experimental approach; performed the ex vivo experiment of WGA-stained mucus (Fig. S2); performed some of the ex vivo experiments and analyzed some of the results in Figs. 2–4 and S3–S7; tested optical properties of test solutions (Fig. S8); codeveloped the theoretical model; developed a computational approach for the theoretical model calculations; cooptimized and coperformed calculations for the theoretical model and coanalyzed results in Fig. 3; developed an approach to extract liquid fraction of murine colonic contents; cowrote the paper.

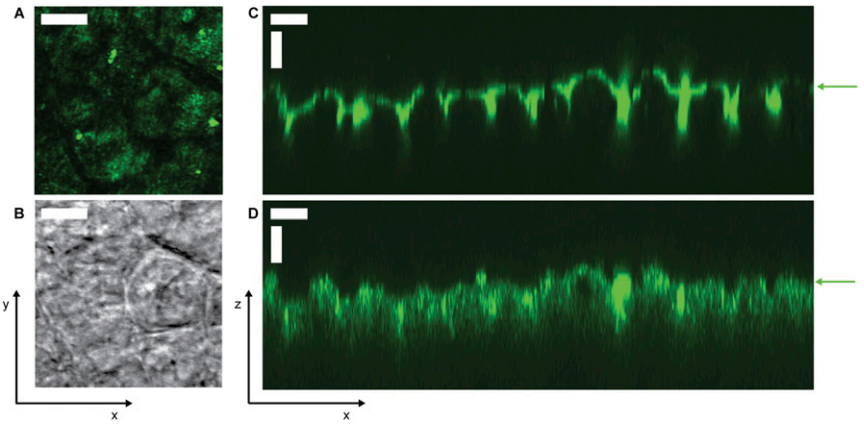

Fig. S1. Images of murine epithelium in the *xy* and *xz* planes. (*A*) Two-photon and (*B*) bright-field micrographs of unwashed epithelium from a mouse fed standard chow, imaged under FC oil. (*C* and *D*) Side views of lectin-stained epithelium washed with saline and imaged under aqueous solutions. Staining was performed by incubating a colon explant with 200 μL of a test solution of 2 mg/mL Rhodamine Ulex Europaeus Agglutinin I (Vector Laboratories), which stains α-L-fucose residues on the surface of epithelial cells, in Hepes buffer in a sealed Petri dish for 10 min at 4 °C, then washing the exposed luminal side with several milliliters of ice-cold 1× PBS. We then immediately imaged the explant surface using (*C*) confocal fluorescence microscopy (543-nm excitation/560-nm long-pass filter) and (*D*) confocal reflectance microscopy (514-nm excitation/505-nm long-pass filter). Epithelial surface is indicated by green arrows, confirming that the position of the epithelium agrees between the different imaging modalities. The adherent mucus hydrogel overlies the epithelium in the direction of increasing *z* above the green arrows. (All scale bars, 30 μm.)

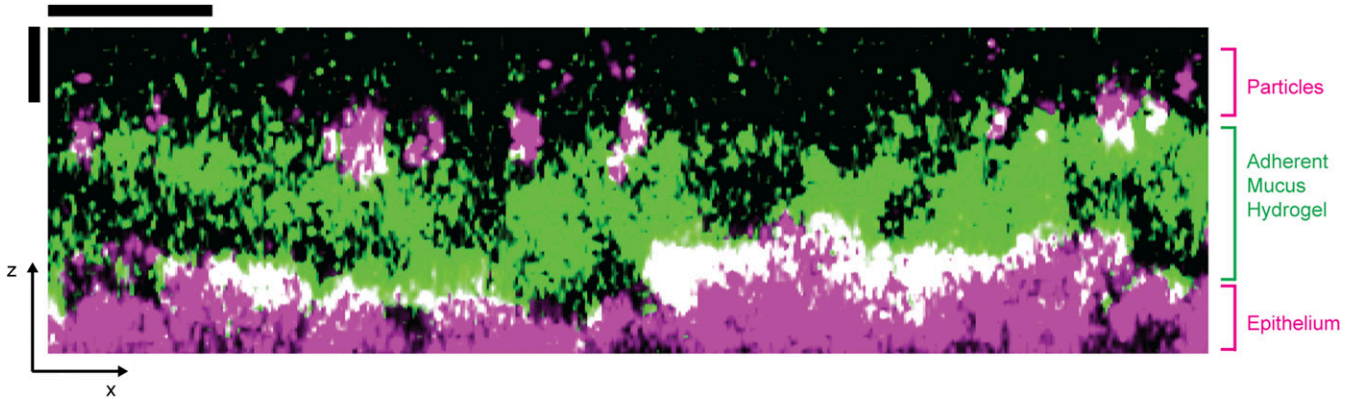

Fig. S2. False-color side view showing wheat germ agglutinin (WGA)-stained adherent mucus hydrogel. We first deposited 1-μm-diameter microparticles onto the explant surface of a freshly excised, washed, and mounted colonic explant. After incubating for 1 h at 4 °C, we then stained the colonic mucus with WGA, a fluorescent lectin that specifically binds to sialic acid sugar residues in the mucins. We prepared 10 μg/mL of WGA-Oregon Green (Invitrogen) in 1× PBS, placed a ∼0.5-mL drop on the exposed surface of the explant, and incubated the sealed Petri dish for 5 min at room temperature. We then washed the exposed surface with several milliliters of ice-cold 1× PBS and immediately imaged the explant surface (lower magenta surface) and the deposited 1-μm microparticles (upper magenta circles) using confocal reflectance microscopy and the stained mucus hydrogel using confocal fluorescence microscopy (488-nm excitation/505-nm long-pass filter). Image is a superimposition of two separate, parallel side views taken at two neighboring positions in the *xy* plane. We observed that the position of the deposited microparticles agrees with the top of the stained mucus hydrogel. (Scale bars, 30 μm.)

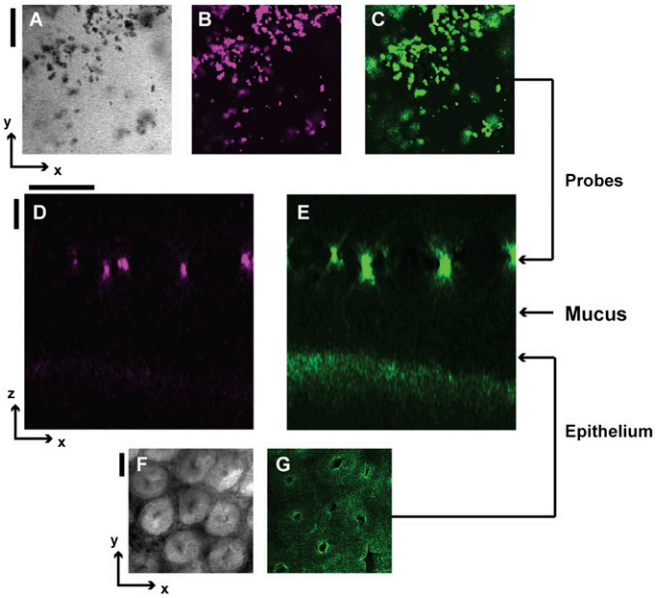

Fig. S3. Colocalization of signal from microparticle probes and epithelium from different imaging modalities. (*A*) Bright field, (*B*) fluorescence excitation, and (*C*) reflectance images of 1-μm probes of the same *xy* slice. (*D*) An *xz* side view of fluorescence signal from 1-μm probes. (*E*) The same *xz* side view as in *D* but of the reflectance signal from 1-μm probes and epithelial surface. (*F*) Bright-field and (*G*) reflectance images of the epithelial surface of the same *xy* slice. The arrow linking *C* to *E* indicates the vertical position of the *xy* slice shown in *A*–*C*. The arrow linking *G* to *E* indicates the vertical position of the *xy* slice shown in *F* and *G*. This confirms that the positions of the microparticles given by confocal reflectance and confocal fluorescence microscopy agree. (Scale bars, 30 μm.)

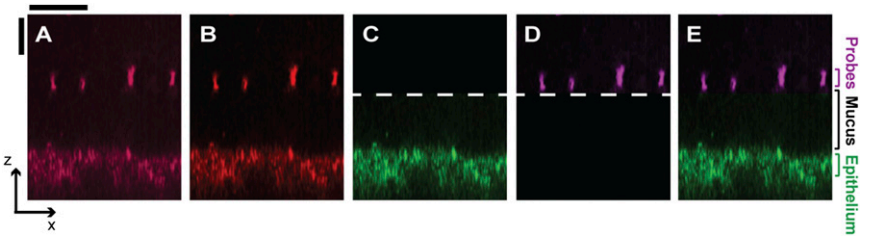

Fig. S4. Overview of image processing of confocal side views. To eliminate artifacts associated with staining and accelerate image acquisition, we used label-free confocal reflectance microscopy to simultaneously image the underlying epithelium (lower surface) and the microparticles deposited on the adherent mucus hydrogel (upper bright spots). To obtain the false-color side views, we first thresholded each side view; *A* shows a representative *xz* side view before processing and *B* shows the image after thresholding, with uniform enhancement of brightness and contrast across the entire image. The image was then split into two parts, and the epithelium was false-colorized green (*C*) and the deposited microparticles or oil–mucus interface (for imaging of unwashed tissues with FC oil) were false-colorized magenta (*D*). Dashed lines indicate where images (*C* and *D*) were split. Merging these two channels produced the side-view images shown, exemplified by *E*. Unless otherwise noted, all of our experiments mapped *z* ranges spanning from below the epithelial surface to well above the mucus hydrogel surface. Each of the side-view images presented in this paper was cropped and scaled in *xz* for clarity (indicated by the *x* and *z* scale bars), to focus on the region corresponding to the mucus hydrogel. (Scale bars, 30 μm.)

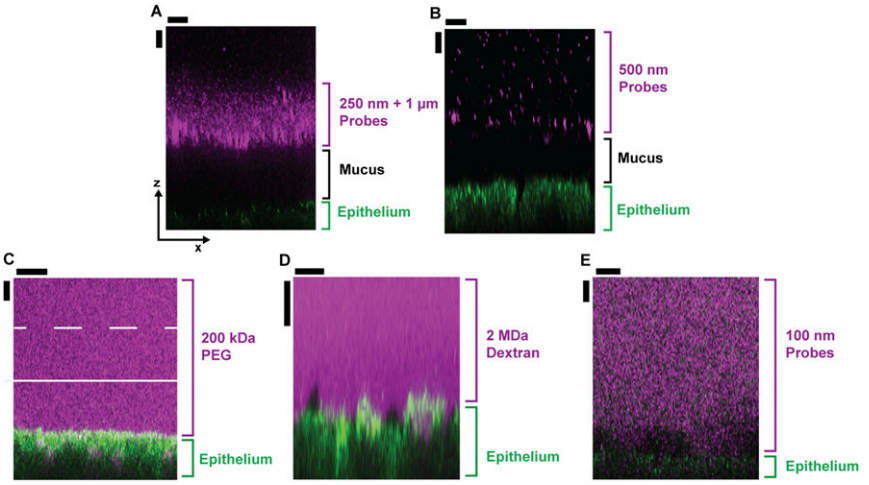

Fig. S5. False-color side views (*xz* plane) of 3D stacks showing probes excluded from (top row) or penetrating (bottom row) the mucus hydrogel. (*A*) Mixture of both 250-nm and 1-μm microparticles and (*B*) 500-nm particles were excluded from the adherent mucus hydrogel. The probes (magenta) were unable to diffuse through the mucus and instead deposited on top of the hydrogel. The probes and the epithelium were simultaneously imaged using (*A*) 514-nm excitation/505-nm long-pass filter and (*B*) 800-nm excitation/650-nm long-pass filter. (*C*) Fluorescent PEG 200 kDa, (*D*) fluorescent dextran 2 MDa, (*E*) fluorescent 100-nm microparticle probes all penetrate the hydrogel. Note that polymers in *A* and *B* were used at concentrations below those that cause mucus compression. The probes (magenta) diffused through the mucus and reached the underlying epithelium (green), except for some isolated regions immediately adjacent to the epithelium observed in some experiments (dark patches). The probes were imaged using confocal fluorescence microscopy (488-nm excitation/505-nm long-pass filter) and the epithelium was imaged using confocal reflectance microscopy. The adherent mucus hydrogel overlies the epithelium in the direction of increasing *z* above the green arrows; solid and dashed white lines in *C* indicate the approximate average and maximal positions of the top of the mucus, measured using 1-μm microparticles. In each experiment using probes of different sizes, after placing the test solution onto the exposed luminal surface, we incubated the tissue at 4 °C for 1–2 h before imaging the explant. We estimated the time required for probes 100 nm or smaller to diffuse through the mucus as being <10 min, and the time required for the 250-nm probes to diffuse across the vertical extent of the mucus in free solution as being ∼10 min, both much shorter than the incubation time. We thus deduce that the fluorescent probes smaller than the measured mucus mesh size had sufficient time to diffuse through the mucus to the underlying epithelium, and that the measured exclusion of the larger probes reflects the presence of the adherent mucus hydrogel. (Scale bars, 30 μm.)

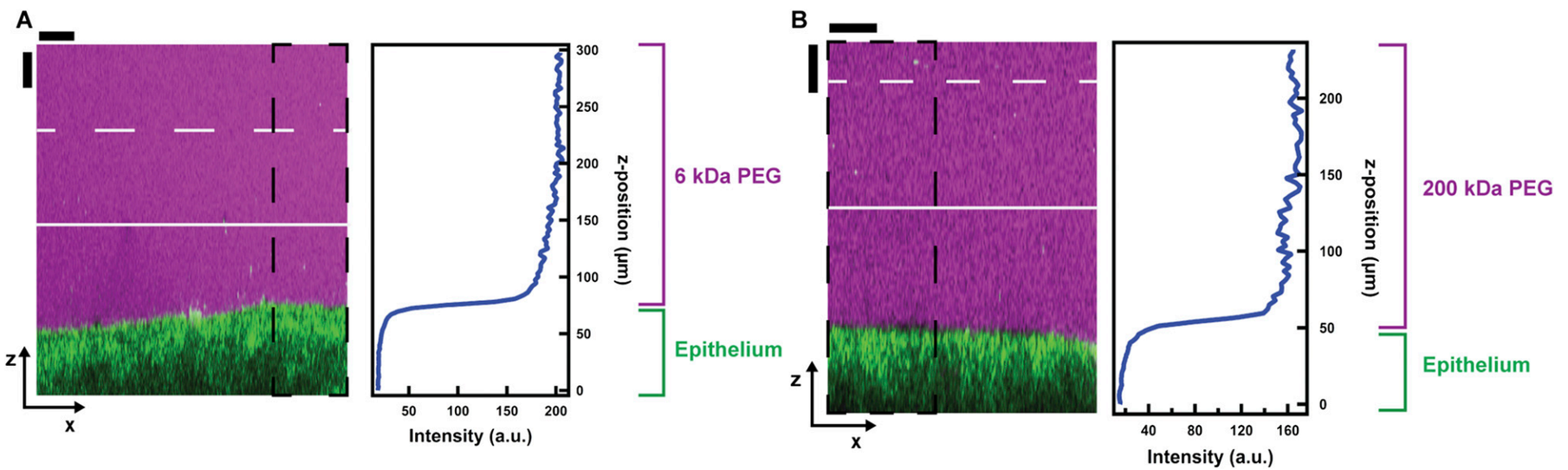

Fig. S6. Side view showing penetration of mucus hydrogel by polymers. The polymer self-diffusion coefficient in the free solution outside the mucus, D_{free}, is represented by D_0 for the dilute polymer solutions and can be estimated as $D_{free} \approx D_0(c/c^*)^{-7/4}$ for the polymer solutions that were above their overlap concentration c^*. Our experiments spanned $D_0 \approx 10^{-11}$ to 3×10^{-10} m^2/s and $c/c^* \approx 0$–10, therefore $D_{free} \approx 2 \times 10^{-13}$ to 3×10^{-10} m^2/s. The characteristic time taken for the polymers to diffuse through the mucus can thus be estimated as ranging from ~1 s to 1 h, shorter than the time taken to perform the experiments. We thus assume that the polymer molecules were able to diffuse through the mucus hydrogel before imaging commenced in all of the experiments. To study the steady-state penetration of the PEG into the adherent mucus hydrogel, we imaged two representative test solutions: (*A*) 13% (wt/vol) PEG 6k spiked with 0.5 mg/mL FITC-PEG 5k and (*B*) 3% (wt/vol) PEG 200k spiked with 0.6 mg/mL FITC-PEG 200k. Consistent with our expectation, in both cases the polymer penetrated through the adherent mucus hydrogel and reached the underlying epithelium. Traces show the spatial variation of the *x*-averaged probes fluorescence intensity for the region indicated by the dashed black box. The probes (magenta) diffused through the mucus and reached the underlying epithelium (green). The probes were imaged using confocal fluorescence microscopy and the epithelium was imaged using confocal reflectance microscopy. The adherent mucus hydrogel overlies the epithelium in the direction of increasing *z* above the epithelium; solid and dashed white lines show the average and maximal positions of the top of the mucus, measured using 1-μm microparticles. (Scale bars, 30 μm.)

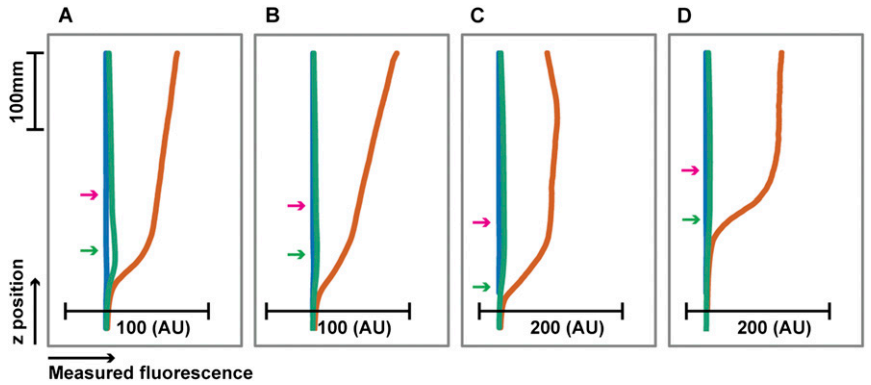

Fig. S7. Fluorescence profiles of test solutions deposited on mucus hydrogel, before and after washing. We expect that the carboxyl groups on the mucin sialic acid residues were negatively charged in our experiments (pH ~7), and therefore complexation between the added PEG and the mucins is minimal. Moreover, we took care not to expose PEG solutions to light and keep them at low temperatures when not in use, to minimize oxidation. To confirm that labeled PEG molecules were not chemically cross-linked to the mucus hydrogel as they diffused through the hydrogel, we performed four sets of fluorescence measurements, using as test solutions (*A*) 5 μM fluorescein, (*B*) 15 μM FITC-PEG 350, (*C*) 6 μM FITC-PEG 5k, and (*D*) 15 μM FITC-PEG 350 in 60% (wt/vol) PEG 400. Four different explants were incubated with 1-μm microparticles for >1 h then imaged using confocal reflectance (to identify epithelial surface and microparticles on mucus) and confocal fluorescence (to quantify fluorescence of deposited test solution). Curves show fluorescence profiles of test solutions: horizontal axis shows measured fluorescence, averaged over a 450-μm × 450-μm *xy* field of view, and the vertical axis shows *z* position. Green and magenta arrows show average positions of epithelial surface and probes deposited on the mucus hydrogel surface. We first used PBS as the test solution to provide a measure of background fluorescence (blue curves). We then deposited dyed test solution on the mucus (orange curves). We then washed the explant with saline (green curves). Fluorescence profiles returned to background levels after washing, suggesting that strong chemical interactions (such as covalent reactions) between the labeled PEG and the mucus hydrogel do not occur. We used the same gain settings before and after.

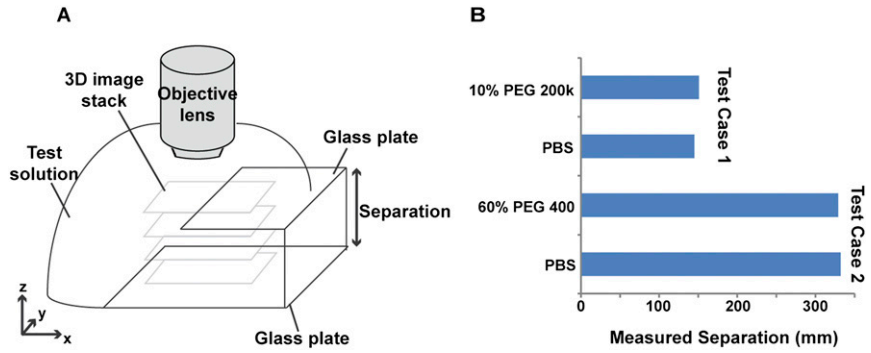

Fig. S8. Optical properties of polymer solutions do not appreciably affect *z* measurements. (*A*) Schematic showing setup of control experiments, measuring separation between two parallel glass plates using the same confocal reflectance microscopy approach. The test solution infiltrated the open gap between the two plates. (*B*) We first quantified separation using PBS as the test solution filling the space between the two plates, and then used either 10% (wt/vol) PEG 200k (test case 1), or 60% (wt/vol) PEG 400 (test case 2) as the test solution. Introduction of the polymer solution did not change the measured *z* separation appreciably, indicating that optical effects due to the presence of the polymer solution did not significantly affect the *z* measurements.

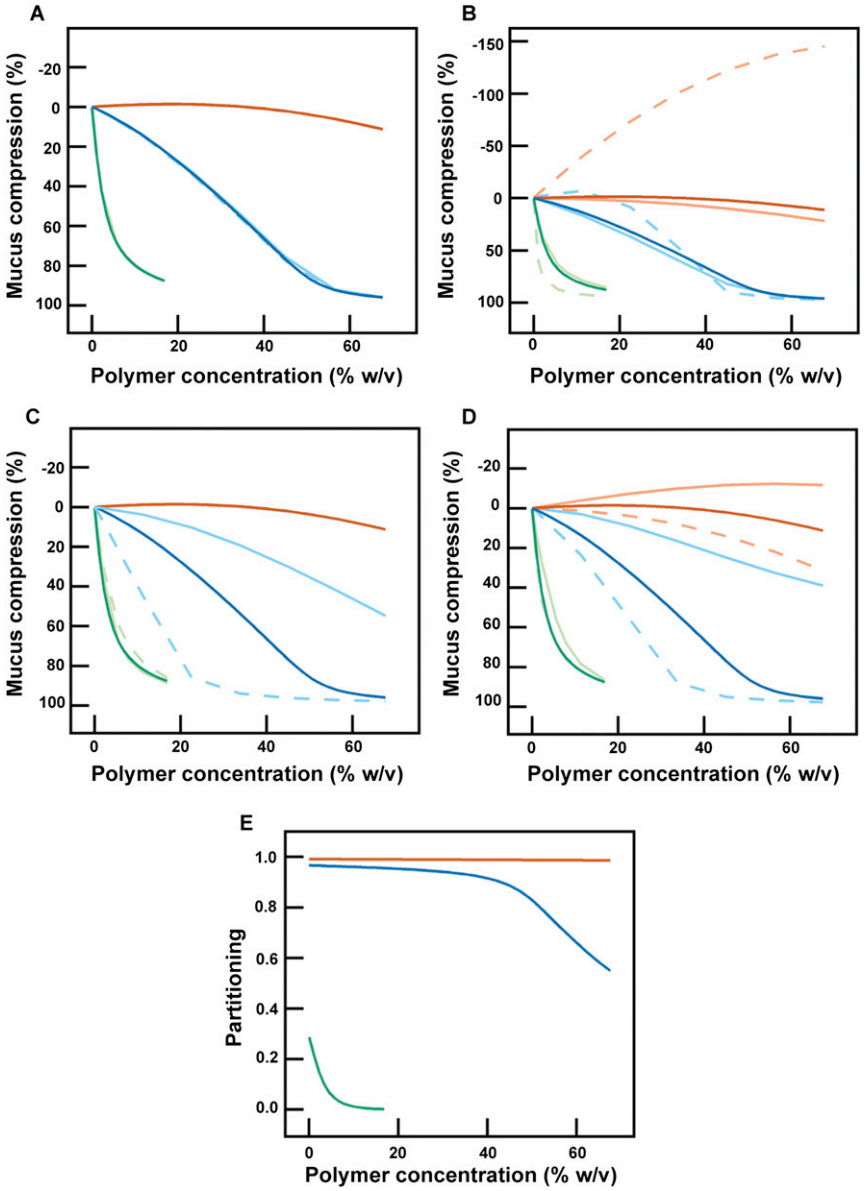

Fig. S9. Sensitivity of model predictions to variations in numerical parameters. Each panel shows numerical calculations (*Materials and Methods*) of the mucus hydrogel compression for different concentrations of PEG 400 (orange), 6k (blue), and 200k (green). Note that due to the constraint derived in the initial polymer-free case, some of the parameters are coupled and cannot be varied independently. (*A*) ν^0_M values are varied and corresponding values of N_M are adjusted to satisfy the initial polymer-free constraint. Light, solid traces correspond to $\nu^0_M = 0.07$ and $N_M = 628$, and light, dashed traces correspond to $\nu^0_M = 0.35$ and $N_M = 2{,}026$. Note the overlap between the solid and dashed traces. (*B*) χ_{SM} values are varied and corresponding values of N_M are adjusted to satisfy the initial polymer-free constraint. Light, solid traces correspond to $\chi_{SM} = -0.2$ and $N_M = 715$, and light, dashed traces correspond to $\chi_{SM} = 0.45$ and $N_M = 9{,}425$. Upper and lower less opaque curves in Fig. 2*A*, which correspond to $\chi_{SM} = 0.1$ and -0.1, were characterized by $N_M = 1{,}247$ and $N_M = 833$. (*C*) The number of Kuhn segments y for each PEG molecule is varied. Light, solid traces correspond to $y = 1$, 2, and 76, and light, dashed traces correspond to $y = 1$, 11, and 611 for PEG 400, 6k, and 200k, respectively. (*D*) χ_{MP} is varied. Light, solid traces correspond to $\chi_{MP} = 0$ and light, dashed traces correspond to $\chi_{MP} = 0.5$. In each panel, the dark solid traces are the simulations presented in Fig. 2*A*. In all cases, we observed similar trends of compression with polymer concentration and molecular weight as in the experiments. (*E*) Numerical calculations showing the partitioning between the hydrogel and solution phase for PEG 400 (orange), 6k (blue), and 200k (green). The ratio of PEG inside and outside the hydrogel (ν_P^{in}/ϕ, denoted "Partitioning") is plotted against the PEG concentration outside the hydrogel. Consistent with our expectation, the higher-molecular-weight polymer is more likely to be excluded from the mucus hydrogel.

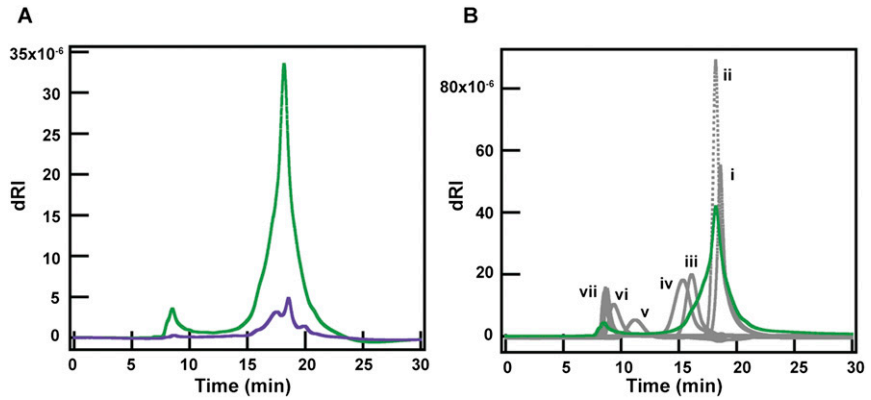

Fig. S10. Gel permeation chromatography of luminal contents from SPF and GF mice. We used an Agilent 1100 HPLC with a binary pump and autosampler, which was connected to a Tosoh TSKgel G3000SWxl column equilibrated with 1× PBS, pH 7.4, flow rate 0.7 mL/min. For detection of the polymers, a Wyatt DAWN HELEOS light scattering instrument with a Wyatt Optilab Rex refractive index detector was used. Detected peaks were analyzed using ASTRA V software. For the pullulan standards, the Agilent PL 2090-0101 Pullulan polysaccharide calibration kit (Agilent) was used. An injection volume of 50 μL was used for each. All samples were prepared in 1× PBS and run through a sterile syringe filter (polyvinylidene fluoride, 13-mm diameter, pore size of 0.22 μm; Fisherbrand) before injection. For luminal contents, on the day of the experiment, frozen liquid fractions were warmed to room temperature for 10–20 min then diluted twofold with 1× PBS. Samples were centrifuged at 12,000 × *g* at 4 °C for 2 h in sterile centrifugal filters (polyvinylidene fluoride, pore size 0.22 μm; EMD Millipore). After centrifugation, samples were allowed to equilibrate to room temperature for 30 min before injection. For all liquid fraction samples, an injection volume of 10 μL was used. If multiple runs were performed on the same sample, the remaining sample volume was stored at 4 °C until prior runs were complete. (*A*) Chromatograms of luminal contents from four 3-mo-old SPF males (purple) and two male and one female, 4-mo-old GF (green) mice. Differential refractive index (dRI) is plotted against time (minutes). Both runs were run on the same day. (*B*) Chromatograms of luminal contents of GF mice (green) and pullulan standards (gray). dRI is plotted against time (minutes). Concentrations and peak average molecular weights of the standards used were (*i*) 5 mg/mL 180 Da, (*ii*) 8 mg/mL 667 Da, (*iii*) 4 mg/mL 6,100 Da, (*iv*) 4 mg/mL 9,600 Da, (*v*) 1 mg/mL 47,100 Da, (*vi*) 1 mg/mL 107,000 Da, (*vii*) 1 mg/mL 194,000 Da, 344,000 Da, and 708,000 Da.